Power and photon budget of a remote phosphor LED module

Paula Acuña,[1,*] Sven Leyre,[1] Jan Audenaert,[1] Youri Meuret,[1] Geert Deconinck,[2] and Peter Hanselaer[1]

[1]*Light and Lighting Laboratory, KU Leuven, Gebroeders De Smetstraat 1, Ghent 9000, Belgium*
[2]*ESAT/ELECTA, KU Leuven, Kasteelpark Arenberg 10, bus 2445, Heverlee 3001, Belgium*
[*]*paula.acuna@kuleuven.be*

Abstract: Light-emitting diodes (LEDs) are becoming increasingly important for general lighting applications. The remote phosphor technology, with the phosphor located at a distance from the LEDs, offers an increased extraction efficiency for phosphor converted LEDs compared to intimate phosphor LEDs where the phosphor is placed directly on the die. Additionally, the former offers new design possibilities that are not possible with the latter. In order to further improve the system efficiency of remote phosphor LEDs, realistic simulation models are required to optimize the actual performance. In this work, a complete characterization of a remote phosphor converter (RPC) consisting of a polycarbonate diffuser plate with a phosphor coating on one side via the bi-directional scattering distribution function (BSDF) is performed. Additionally, the bi-spectral BSDF which embraces the wavelength conversion resulting from the interaction of blue light with the RPC is determined. An iterative model to predict the remote phosphor module power and photon budget, including the recuperation of backward scattered light by a mixing chamber, is introduced. The input parameters for the model are the bi-spectral BSDF data for the RPC, the emission of the blue LEDs and the mixing chamber efficiency of the LED module. A good agreement between experimental and simulated results was found, demonstrating the potential of this model to analyze the system efficiency with errors smaller than 4%.

OCIS codes: (290.1483) BSDF, BRDF, and BTDF; (230.3670) Light-emitting diodes; (260.2510) Fluorescence; (290.0290) Scattering.

References and links

1. S. Pimputkar, J. S. Speck, S. P. DenBaars, and S. Nakamura, "Prospects for LED lighting," Nat. Photonics **3**(4), 180–182 (2009).
2. A. Keppens, P. Acuña, H. Chen, G. Deconinck, and P. Hanselaer, "Efficiency evaluation of phosphor-white high-power light-emitting diodes," J. Light Vis. Env. **35**(3), 199 (2011).
3. N. Narendran, Y. Gu, J. P. Freyssinier-Nova, and Y. Zhu, "Extracting phosphor-scattered photons to improve white LED efficiency," Phys. Status Solidi A **202**(6), R60–R62 (2005).
4. H. Huang, Y. Huang, and C. Tsai, "Planar Lighting System Using Array of Blue LEDs to Excite Yellow Remote Phosphor Film," J. Disp. Technol. **7**(1), 44–51 (2011).
5. M. Lin, S. Ying, M. Lin, K. Tai, S. Tai, C. Liu, J. Chen, and C. Sun, "Ring Remote Phosphor Structure for Phosphor-Converted White LEDs," IEEE Photon. Technol. Lett. **22**(8), 574–576 (2010).
6. Y. Zhu and N. Narendran, "Optimizing the Performance of Remote Phosphor LEDs," J. Light Vis. Env. **32**(2), 115–119 (2008).
7. H. C. Kuo, C. W. Hung, H. C. Chen, K. J. Chen, C. H. Wang, C. W. Sher, C. C. Yeh, C. C. Lin, C. H. Chen, and Y. J. Cheng, "Patterned structure of remote phosphor for phosphor-converted white LEDs," Opt. Express **19**(S4 Suppl 4), A930–A936 (2011).
8. P. Yuen, H. Shiung, and M. Devarajan,IEEE, ed., "Influence of phosphor packaging configurations on the optical performance of Chip on Board phosphor converted Warm White LEDs," in *Proceedings of 5th Annual Symposium on Quality Electronic Design, International Society for Quality Electronic Design*, ed. (IEEE, 2013), pp. 329–333.

#209148 - $15.00 USD Received 1 Apr 2014; revised 20 May 2014; accepted 21 May 2014; published 2 Jun 2014

9. C. Hoelen, H. Borel, J. de Graaf, M. Keuper, M. Lankhorst, C. Mutter, L. Waumans, and R. Wegh, “Remote phosphor LED modules for general illumination: toward 200 lm/W general lighting LED light sources,” Proc. SPIE **7058**, 70580M (2008).
10. I. U. Perera and N. Narendran, “Thermal management of the remote phosphor layer in LED systems,” Proc. SPIE **8835**, 883504 (2013).
11. A. Keppens, Y. Ohno, G. Deconinck, and P. Hanselaer, “Determining phosphors' effective quantum efficiency for remote phosphor type LED modules,” presented at the Tutorial and Expert Symposium on Spectral and Imaging Methods for Photometry and Radiometry, Bern, Switzerland, 30 July-2 August (2010).
12. H. Xiao, Y.-J. Lu, T.-M. Shih, L.-H. Zhu, S.-Q. Lin, P. J. Pagni, and Z. Chen, “Improvements on Remote Diffuser-Phosphor-Packaged Light-Emitting Diode Systems,” IEEE Photon. J. **6**(2), 1–8 (2014).
13. K. Yamada, Y. Imai, and K. Ishii, “Optical Simulation of Light Source Devices Composed of Blue LEDs and YAG Phosphor,” J. Light Vis. Env. **27**(2), 70 (2003).
14. Y. Zhu and N. Narendran, “Investigation of Remote-Phosphor White Light-Emitting Diodes with Multi-Phosphor Layers,” Jpn. J. Appl. Phys. **49**(10 10R), 100203 (2010).
15. R. Hu and X. Luo, “A Model for Calculating the Bidirectional Scattering Properties of Phosphor Layer in White Light-Emitting Diodes,” J. Lightwave Technol. **30**(21), 3376–3380 (2012).
16. R. Hu, Y. Wang, Y. Zou, X. Chen, S. Liu, and X. Luo, “Study on phosphor sedimentation effect in white light-emitting diode packages by modeling multi-layer phosphors with the modified Kubelka-Munk theory,” J. Appl. Phys. **113**(6), 063108 (2013).
17. R. Hu, H. Zheng, J. Hu, and X. Luo, “Comprehensive Study on the Transmitted and Reflected Light Through the Phosphor Layer in Light-Emitting Diode Packages,” IEEE J. Disp. Technol. **9**(6), 447–452 (2013).
18. C. Sommer, P. Hartmann, P. Pachler, H. Hoschopf, and F. P. Wenzl, “White light quality of phosphor converted light-emitting diodes: A phosphor materials perspective of view,” J. Alloy. Comp. **520**, 146–152 (2012).
19. C. H. Hung and C. H. Tien, “Phosphor-converted LED modeling by bidirectional photometric data,” Opt. Express **18**(S3 Suppl 3), A261–A271 (2010).
20. P. Hanselaer, A. Keppens, S. Forment, W. R. Ryckaert, and G. Deconinck, “A new integrating sphere design for spectral radiant flux determination of light-emitting diodes,” J. Meas. Sci. Technol. **20**(9), 095111 (2009).
21. ASTM Standard E1392, 1996(2002), Standard Practice for Angle Resolved Optical Scatter Measurements on Specular or Diffuse Surfaces, 2002.
22. F. E. Nicodemus, “Geometrical considerations and nomenclature for reflectance,” in *Radiometry.* E. D. Jones and Bartlett Publishers Inc, ed. (Academic, 1992).
23. F. B. Leloup, S. Forment, P. Dutré, M. R. Pointer, and P. Hanselaer, “Design of an instrument for measuring the spectral bidirectional scatter distribution function,” Appl. Opt. **47**(29), 5454–5467 (2008).
24. A. Keppens, W. R. Ryckaert, G. Deconinck, and P. Hanselaer, “High power light-emitting diode junction temperature determination from current-voltage characteristics,” Appl. Phys. (Berl.) **104**(9), 093104 (2008).
25. N. C. George, K. A. Denault, and R. Seshadri, “Phosphors for solid-state white lighting,” Annu. Rev. Mater. Res. **43**(1), 481–501 (2013).
26. Intematix Corp., “Silicate Product Family,” in Brochure Intematix Corporation, 2013.

1. Introduction

Light-emitting diodes (LEDs) are commonly used in general lighting applications because of their outstanding characteristics such as high efficacy, environmental friendliness, and long lifetime [1]. Two main approaches to create white light with LEDs can be identified: a combination of monochromatic LEDs (commonly red, green, and blue) on the one hand, and the excitation of a yellow phosphor using blue LEDs on the other hand, i.e. phosphor converted LEDs (pc-LEDs). The performance of the former approach is however limited due to the significantly lower quantum efficiency of green LEDs compared to the blue ones (green: <10%, blue: 35%) [1]. For conventional pc-LEDs, the power losses in order of importance are: the LED die internal quantum efficiency, package efficiency, phosphor quantum efficiency and Stokes shift of the phosphor [2]. Regarding the package efficiency, one has to consider the photon absorption by the chip and the package due to the back-scattering of the photons emitted by the phosphor. To minimize this effect, the scattered photon extraction method (SPE) has been proposed in 2005 [3]. With the SPE, back-scattered light can be recuperated by locating the phosphor at a remote distance from the chip, which increases the probability of back-scattered light to interact with a reflective surrounding. This method promises an enhancement of up to 40% in light extraction efficiency when implemented at package level [3]. Moreover, the remote phosphor technology suppresses angular color variations, thus improving the color quality and luminous efficiency [4].

The remote phosphor concept has been applied not only to the single die package [3,5–7], but also to the chip on board (CoB) package [8] and to LED modules [9] (see Fig. 1).

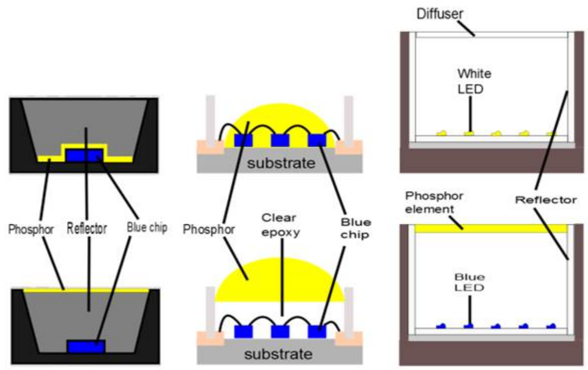

Fig. 1. Intimate white phosphor converted LEDs (upper row) and remote phosphor concept (lower row) applied to: single die package (left), chip on board package (middle), and module (right).

For the CoB approach the luminous efficacy of the remote phosphor concept has been reported to be lower than with the intimate phosphor concept [8]. This is due to the phosphor's thermal quenching triggered by the higher operating temperature despite the remote location. The increased temperature of the phosphor is the result of a high thermal resistance between the phosphor and the heatsink [8]. Regarding the LED module, the remote phosphor concept has the advantage to withstand high case temperatures with a low drop in the wall plug efficiency (WPE) (−0.10% WPE/°C for remote phosphor versus −0.18% WPE/°C for intimate phosphor) [9]. Yet the efficacy for the remote phosphor concept applied to modules currently reaches 80 lm/W, while the theoretical limit is 180 lm/W [9]. Apart from [9–12], the literature contributing to the understanding of the optical and thermal behavior of the remote phosphor concept applied to the LED modules is very limited.

To further improve the system efficiency, a good understanding of the optical behavior of a white LED module is necessary. Attempts to model the phosphor element of a single die LED with intimate YAG phosphor have been reported in [13,14]. The reflected and transmitted flux of the "blue" excitation photons and the "yellow" emitted photons have been measured using two integrating spheres. The Kubelka-Munk theory, complemented with the wavelength conversion phenomena, has also been used to predict the backward and forward scattering of a phosphor film as a function of the thickness, phosphor concentration and particle size assuming homogeneous concentration [15] and gradients of concentration across the thickness [16,17]. In [18] a ray tracing model based on Mie theory using the microscopic parameters of the phosphor and the embedding matrix was defined. These models either do not consider the angular dependence in the scattering process, or require many microscopic parameters, which are hard to acquire. In [19] the interaction of phosphor emission and scattering of a single die package with intimate phosphor are characterized by measuring the bi-directional scattering distribution function (BSDF) of the phosphor. However, only the normalized luminous intensity distribution and the color point have been predicted.

This work tackles the optical characterization and modeling of a remote phosphor LED module, whose constituent elements are the blue LED packages, the mixing chamber and a remote phosphor converter (RPC). The RPC consists of a polycarbonate diffuser plate with a Eu doped silicate phosphor coating on one side. Typically, the phosphor coating contains a blend of phosphor powder (Garnets, Silicates) and a binder (polyacrylate, cellulose). Besides the surface and volume scattering by the phosphor blend, modeling the surface and volume scattering by the diffuser must also be taken into account. As such, the resulting optical model comprises of: the optical power of the blue LED packages, the module geometry, the mixing chamber (MC) optical reflectance properties, and the wavelength dependent scattering of the phosphor converter, the latter being far most complex.

The determination of the BSDF and the total integrated scattering (TIS) of the RPC for “blue” and “yellow” incident light, including elastic scattering and wavelength conversion, is essential. In what follows, the blue LED radiation will be designated by “blue”, while the emission spectrum of the phosphor will be designated by “yellow”. From the BSDF, the power and photon budget of the RPC and the complete remote phosphor LED module are determined and validated. The BSDF of the RPC will be dependent on the thickness and concentration of the phosphor coating. However, this paper concentrates on the light extraction efficiency of the module and the interaction between the RPC and the MC. The optimization of the RPC itself, which is commercially available and representative for remote phosphor applications, has not been subject of our investigation. The structure of this paper is as follows. Section 2 describes the experiments carried out for the characterization of the MC and the RPC. In section 3 the experimental results of the MC characterization are presented. A mathematical description of the RPC characterization is explained in section 4. Power and photon budget of the RPC are computed and validated with experimental results in sections 5 and 6, respectively. Finally section 7 discusses the conclusions and future work.

2. Experiments

A remote phosphor LED module was assembled as follows. The MC is chosen to be cylindrical with a radius of 35 mm and a height of 43 mm. The inner surface of the MC is covered with Mylar Polyethylene terephthalate (MPET) (Fig. 2). On the base of the MC four InGaN blue LEDs LuxeonStar of 0.84 W are mounted. The outer surface of the base has been mounted on a heatsink. The RPC is mounted on top of the MC, with the phosphor coating facing the MC.

The spectral radiant flux $\Phi_{e,\lambda}$ of both the MC and the MC with the RPC are measured using a custom-made integrating sphere [20]. The RPC is characterized by measuring the BSDF. The monochromatic BSDF is defined as the ratio of the differential spectral radiance of the sample at a particular viewing angle to the differential spectral irradiance on the sample from a particular incident solid angle [21]:

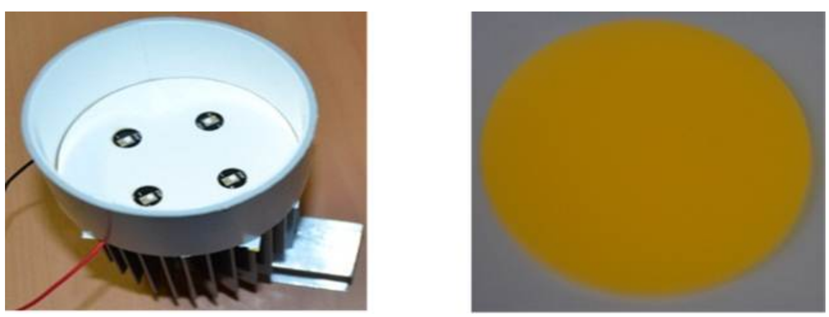

Fig. 2. Mixing Chamber with blue LEDs (left) and remote phosphor converter (right).

$$q_e(\theta_i,\phi_i,\theta_s,\phi_s) = \frac{dL_{e,\lambda,s}(\theta_i,\phi_i,\theta_s,\phi_s)}{dE_{e,\lambda,i}(\theta_i,\phi_i)}\left[\frac{1}{sr}\right] \quad (1)$$

where $dL_{e,\lambda,s}$ is the differential spectral radiance emitted by the sample in direction (θ_s,ϕ_s), and $dE_{e,\lambda,i}$ the differential spectral irradiance that illuminates the sample from direction (θ_i,ϕ_i). The angles $(\theta_i,\phi_i,\theta_s,\phi_s)$ are given in spherical coordinates and are referred to the normal of the sample.

#209148 - $15.00 USD Received 1 Apr 2014; revised 20 May 2014; accepted 21 May 2014; published 2 Jun 2014

When the RPC is exposed to radiation which overlaps with the excitation spectrum of the material, elastic scattering (without wavelength conversion) and scattering with wavelength conversion towards both sides of the RPC occur, as illustrated in Fig. 3.

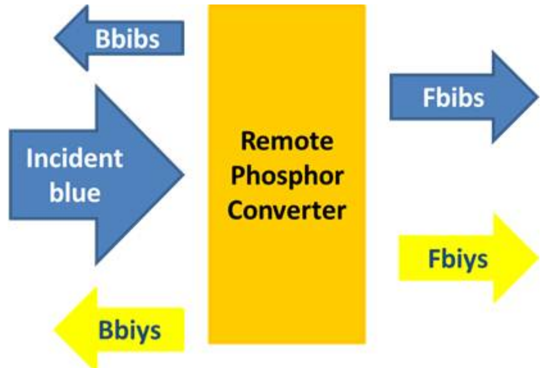

Fig. 3. Elastic scattering (no wavelength conversion) and scattering with wavelength conversion both occur in the RPC when it is illuminated with short-wavelength radiation within the excitation region. ‘B’ and ‘F’ stand for backwards and forwards scattering, ‘b’ and ‘y’ for blue and yellow, ‘i’ and ‘s’ for incident and scattered, respectively.

However, the monochromatic BSDF defined by Eq. (1) cannot be used to describe wavelength conversion [22]. To extend Nicodemus’ definition for the cross-wavelength energy transfer, the contribution of each discrete incident wavelength within the excitation range to each scattered wavelength at a certain direction (θ_s, ϕ_s) has to be considered. This will be called the bi-spectral BSDF, due to the fact that scattering at one wavelength λ_s can be originating from several incident wavelengths λ_i. Mathematically expressed, the bi-spectral BSDF $q_{e,\lambda}(\theta_i, \phi_i, \theta_s, \phi_s, \lambda_i, \lambda_s)$ can be defined as the derivative of the monochromatic BSDF to the incident wavelength:

$$q_{e,\lambda}(\theta_i, \phi_i, \theta_s, \phi_s, \lambda_i, \lambda_s) = \frac{dq_e}{d\lambda_i}\left[\frac{1}{sr \cdot nm}\right] \tag{2}$$

As the bi-spectral BSDF of the RPC depends on both the incident and scattered wavelengths, it becomes very cumbersome to implement a detailed spectral simulation scheme. To simplify the simulation of the remote phosphor LED module, a two wavelength approximation is adopted where the blue emission from the LED is represented by one wavelength and the yellowish emission of the RPC by another.

Both the monochromatic BSDF as well as the bi-spectral BSDF are measured with a custom-made setup. A schematic illustration of the setup is presented in Fig. 4. The illumination part consists of a Xe-lamp with secondary optics to create a wide collimated light bundle (diameter of 14 mm), interference filters to adjust the spectrum and a set of neutral density filters to increase the dynamic range. The detection unit consists of a detector head connected with an optical fiber to a spectrometer with CCD. The detector’s head has a circular aperture with adjustable diameter of maximum 25.4 mm and is positioned at a distance of 886 mm from the measured sample, resulting in a maximum solid angle of 6.25×10^{-4} sr. The detector head can be rotated around the central sample holder using two rotation stages. A more elaborate description of the experimental setup can be found in [23].

To characterize the RPC, an interference filter (450 nm - 470 nm) was positioned into the light path to measure the angular distribution of the non-converted blue and the converted yellow light for incident blue light. On the other hand, the interaction of the RPC with incident yellow light showing no wavelength conversion is measured by inserting a cut-on filter into the light path of the incident beam (cut-on wavelength of 475 nm).

#209148 - $15.00 USD Received 1 Apr 2014; revised 20 May 2014; accepted 21 May 2014; published 2 Jun 2014

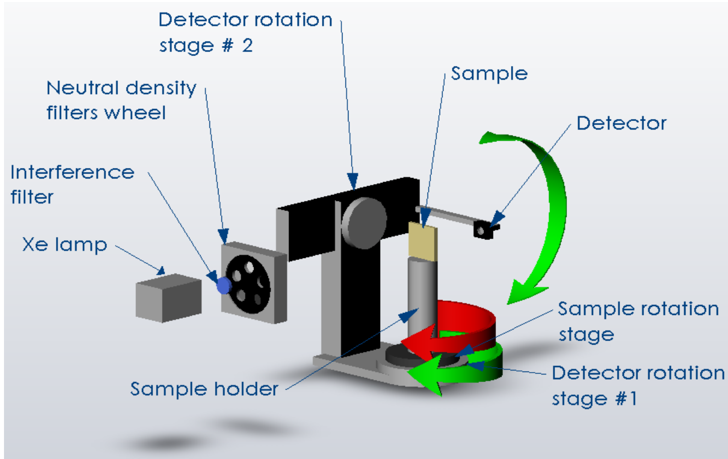

Fig. 4. Measurement setup of the bidirectional scattering distribution function.

The incident angle can be adjusted by rotating the sample with the sample rotation stage. For each incident angle (θ_i = 5°, 45°, 56°) the measurements are conducted for the scattered angles $0° \le \theta_s \le 90°$ in the incident plane, both in reflection (backward) and transmission (forward), and for azimuthal angles $-60° \le \phi_s \le 60°$ in the plane perpendicular to the incident plane and through the specular direction.

3. Characterization of the mixing chamber (MC)

The LEDs were driven at a constant direct current of 200 mA while monitoring the forward voltage and the junction temperature variation. The ambient temperature was 25 °C ± 2 °C and the forward voltage varied no more than 5 mV, which guarantees a junction-temperature variation smaller than 3 K [24]. The emission peak for the blue LEDs in the MC is 451 nm, with a Full Width at Half Maximum (FWHM) of 18 nm. In order to study the impact of the cylindrical wall of the MC on the photon and power output, the spectral flux of the blue LEDs mounted on the base, but without the cylindrical wall, was measured first. The spectral power is integrated over the complete spectrum. In a similar way, the total photon flux has been determined. From Table 1, it can be concluded that the blue LEDs convert the electrical power into an optical power with an efficiency of 46%, which is in agreement with the value declared by the manufacturer (45%).

The efficiency of the MC, calculated as the ratio of the radiated power by the MC to the radiated power by the base only, is 0.94. The 6% loss is attributed to the non-ideal reflectance of the MPET material, the multiple reflections in the chamber and the re-absorption by the blue LEDs.

Table 1. Radiometric and photometric characteristics of the blue LEDs and the MC

	Base with blue LEDs	*Base with blue LEDs and wall*
Electrical power [W]	2.2	2.2
Radiated power [W]	0.98	0.92
Efficiency [%]	45.7	41.3
Photon flux [photons/s]	2.2e18	2.1e18

4. Characterization of the remote phosphor converter (RPC)

The excitation and emission spectra of the RPC have been measured with a fluorescence spectrometer Edinburgh FLS920 at an angle of 45° with respect to the normal of the sample. The results are presented in Fig. 5. With an excitation wavelength of 460 nm, the emission is maximal at 600 nm. An emitted wavelength of 620 nm is produced most efficiently by an excitation near 460 nm. Although the noisy signal hampers a straightforward conclusion, the excitation and emission spectra clearly overlap. This will lead to re-absorption of the emitted light in the RPC.

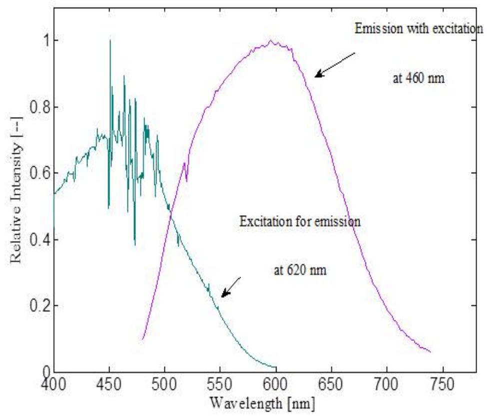

Fig. 5. Excitation and emission spectrum of the RPC CL-830.

4.1 Blue incident, blue scattered (bibs): elastic scattering

The monochromatic BSDF values describing the elastic scattering can be determined according to Eq. (1).

The incident spectrum between 450 nm and 470 nm mimics the incident blue LED spectrum. For any wavelength within the incident spectrum, the scattered light is measured with the rotating detector. The BSDF values at $\lambda = 460nm$ are presented in Fig. 6 as a function of the scattered polar angle in the incident plane, for reflection and transmission.

It is clear that the bi-directional reflectance distribution function (BRDF) shows a specular and a diffuse component, whereas the bi-directional transmittance distribution function (BTDF) exhibits a rather diffuse transmission. The specular component increases with the angle of incidence, similar to Fresnel's laws.

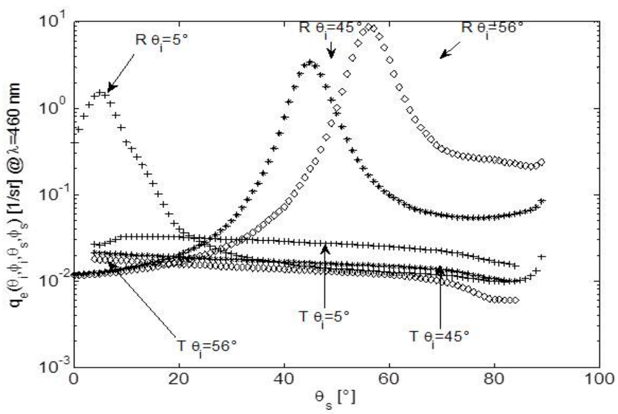

Fig. 6. Forward (T) and backward (R) BSDF values at 460 nm of the RPC CL830 for three angles of incidence (5°, 45°and 56 °).

BRDF and BTDF values have been determined at wavelength within the incident spectrum with a resolution of 0.5 nm. In the approach presented in this paper, a weighted

#209148 - $15.00 USD Received 1 Apr 2014; revised 20 May 2014; accepted 21 May 2014; published 2 Jun 2014

mean value of the monochromatic BSDF $q_e(\theta_i, \phi_i, \theta_s, \phi_s, \lambda)$ over the spectrum of the blue LEDs is introduced as follows.

The spectral radiance at any wavelength can be written as:

$$L_{e.\lambda} = q_e(\lambda) \cdot E_{e,\lambda}(\lambda) \quad (3)$$

Integration over the incident blue spectrum results in a value for the radiance and a definition of the weighted mean blue-blue BSDF value $\langle q_e \rangle_{\Lambda_i=blue,\Lambda_s=blue}$

$$L_e = \sum_{450}^{470} q_e(\lambda) \cdot E_{e,\lambda} \cdot \Delta\lambda = \langle q_e \rangle_{\Lambda_i=blue,\Lambda_s=blue} \cdot \sum_{450}^{470} E_{e,\lambda} \cdot \Delta\lambda \quad (4)$$

With the weighted mean blue-blue BSDF given by

$$\langle q_e \rangle_{\Lambda_i=blue,\Lambda_s=blue} = \frac{\sum_{450}^{470} q_e(\theta_i, \phi_i, \theta_s, \phi_s, \lambda) \cdot E_{e,\lambda}(\theta_i, \phi_i, \lambda) \cdot \Delta\lambda}{\sum_{450}^{470} E_{e,\lambda}(\theta_i, \phi_i, \lambda) \cdot \Delta\lambda} \quad (5)$$

In this equation, only the relative or normalized incident spectrum of the blue pump LED is needed. The weighted mean blue-blue BSDF values for an incident angle of 45° in the incident plane are shown in Fig. 7.

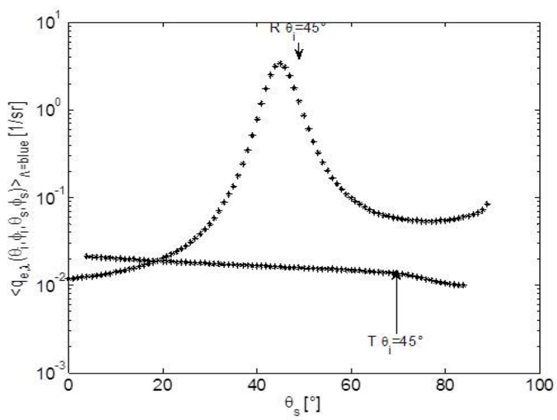

Fig. 7. Weighted average blue-blue BSDF over the range (λ = 450 nm – 470 nm) for backward and forward directions.

The mean BSDF value over the blue region is very similar to the result for a single wavelength (shown in Fig. 6) due to the low wavelength dependency of the monochromatic BSDF.

The total integrated scattered flux (TIS) can be expressed for each hemisphere as:

$$TIS_{bibs} = \frac{\Phi_{e,s}}{\Phi_{e,i}} \quad (6)$$

with $\Phi_{e,s}$ the total scattered flux and $\Phi_{e,i}$ the total incident flux. Considering the definition of radiance, the TIS can be calculated from the weighted mean blue-blue BSDF value $\langle q_e \rangle_{\Lambda_i=blue,\Lambda_s=blue}$:

$$TIS_{bibs} = \sum_{0}^{2\pi} \sum_{0}^{\pi/2} \langle q_e \rangle_{\Lambda_i=blue,\Lambda_s=blue} \cdot \cos\theta_s \cdot \sin\theta_s \cdot \Delta\theta_s \cdot \Delta\phi_s \quad (7)$$

#209148 - $15.00 USD Received 1 Apr 2014; revised 20 May 2014; accepted 21 May 2014; published 2 Jun 2014

Calculation of these values for an incident direction of $(\theta_i = 45°, \phi_i = 0°)$ in the backward and forward direction results in 10.9% and 5.4% of the incident power, respectively (Table 2).

Table 2. Total Integrated Scatter and Absorbed Power (second column) and photons (third column) by the elastic scattering and scattering with wavelength conversion of blue and yellow light with the phosphor RPC (45° angle of incidence).

	[%] initial power	*[%] initial photons*
B*bibs*	10.9	10.9
F*bibs*	5.4	5.4
B*biys*	26.3	33.9
F*biys*	25.7	33.1
Blue losses	32.7	16.7
B*yiys*	45.7	45.7
F*yiys*	47.1	47.1
Yellow lossses	7.2	7.2

4.2 Yellow incident, yellow scattered (yiys): elastic scattering

To optimize the efficiency of the remote phosphor LED module, it is important to recycle the back-scattered yellow light. From Fig. 5, it can be deduced that the emission starts approximately at 470 nm. Therefore, it is necessary to characterize the response of the RPC to these wavelengths. For any wavelength within the incident spectrum, the scattered light is measured the same way as described for the *bibs* interaction. It is evident that in this case some wavelength conversion will take place due to the overlap between the excitation and emission spectra of the phosphor. However, the low absorption of the RPC in this overlap region allows us to still use the monochromatic BSDF approach. The weighted mean yellow-yellow BSDF value has been calculated similar to Eq. (5):

$$\langle q_e \rangle_{\Lambda_i = yellow, \Lambda_s = yellow} = \frac{\sum_{470}^{740} q_e(\theta_i, \phi_i, \theta_s, \phi_s, \lambda) \cdot E_{e,\lambda}(\theta_i, \phi_i, \lambda) \cdot \Delta\lambda}{\sum_{470}^{740} E_{e,\lambda}(\theta_i, \phi_i, \lambda) \cdot \Delta\lambda} \tag{8}$$

The results are shown in Fig. 8 for an incident angle of 45°.

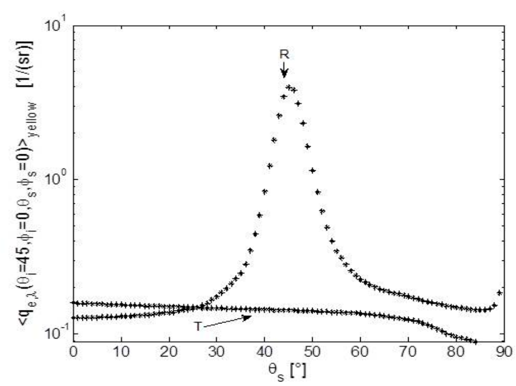

Fig. 8. Forward (T) and backward (R) scattering of yellow light when yellow light is incident (yiys) on the RPC Intematix CL830 (λ = 475 nm – 780 nm).

As it is observed, the behavior of *yiys* is very similar to the interaction *bibs*. The TIS calculation from $\langle q_e \rangle_{\Lambda_i = yellow, \Lambda_s = yellow}$ instead gives 46% and 47% of the incident power for the backward and forward direction, respectively, and a direct loss of 7.2% (see Table 2). Note that a portion of the backward scattering will be recuperated by the MC.

#209148 - $15.00 USD Received 1 Apr 2014; revised 20 May 2014; accepted 21 May 2014; published 2 Jun 2014

4.2 Blue incident, yellow scattered (biys): inelastic scattering

The scattered yellow light at a particular wavelength and viewing angle is caused by all wavelengths present within the incident spectrum. In this case, the incident spectrum between 450 nm and 470 nm is mimicking the incident blue LED spectrum. When integrating Eq. (2), a weighted mean BSDF $\left\langle q_{e,\lambda}\left(\theta_i,\phi_i,\theta_s,\phi_s,\lambda_s\right)\right\rangle_{\Lambda_i=blue}$ at a scattered wavelengths can be defined by Eq. (9):

$$L_{e,\lambda}(\lambda_s)=\sum_{450}^{470} q_{e,\lambda}\cdot E_{e,\lambda}\cdot\Delta\lambda_i=\left\langle q_{e,\lambda}\left(\theta_i,\phi_i,\theta_s,\phi_s,\lambda_s\right)\right\rangle_{\Lambda_i=blue}\cdot\sum_{450}^{470} E_{e,\lambda}\cdot\Delta\lambda_i \tag{9}$$

with the blue weighted mean BSDF given by Eq. (10):

$$\left\langle q_{e,\lambda}\left(\theta_i,\phi_i,\theta_s,\phi_s,\lambda_s\right)\right\rangle_{\Lambda_i=blue}=\frac{\sum_{450}^{470} q_{e,\lambda}\cdot E_{e,\lambda}\cdot\Delta\lambda_i}{\sum_{450}^{470} E_{e,\lambda}\cdot\Delta\lambda_i} \tag{10}$$

This value is measured at any yellow scattered wavelength and at any scattered angle for the particular incident spectrum.

The bi-spectral BSDF in reflection and transmission shows lambertian behavior typical of scattering when wavelength conversion is involved. In contrast with the elastic interactions, no peak at the specular direction is present in reflection.

The two wavelength approach for the *biys* interaction must be completed by taking the mean value of the blue weighted mean $\left\langle q_{e,\lambda}\left(\theta_i,\phi_i,\theta_s,\phi_s,\lambda_s\right)\right\rangle_{\Lambda_i=blue}$ over the different wavelengths in the emission spectrum of the phosphor. This is rather analogous to the blue-blue and yellow-yellow approach described in the paragraphs before.

Indeed, the radiance at any scattered angle can be determined by integrating the spectral radiance given in Eq. (9) over the yellow range:

$$\begin{aligned} L_e &= \sum_{470}^{740}\left\langle q_{e,\lambda}\left(\theta_i,\phi_i,\theta_s,\phi_s,\lambda_s\right)\right\rangle_{\Lambda_i=blue}\cdot E_e\cdot\Delta\lambda_s \\ &= \left\langle\left\langle q_{e,\lambda}\left(\theta_i,\phi_i,\theta_s,\phi_s\right)\right\rangle_{\Lambda_i=blue}\right\rangle_{\Lambda_s=yellow}\cdot E_e\cdot\Delta\Lambda_s \end{aligned} \tag{11}$$

With $\left\langle\left\langle q_{e.\lambda}\left(\theta_i,\phi_i,\theta_s,\phi_s\right)\right\rangle_{\Lambda_i=blue}\right\rangle_{\Lambda_s=yellow}$ equal to:

$$\left\langle\left\langle q_{e.\lambda}\left(\theta_i,\phi_i,\theta_s,\phi_s\right)\right\rangle_{\Lambda_i=blue}\right\rangle_{\Lambda_s=yellow}=\frac{\sum_{470}^{740}\left\langle q_{e,\lambda}\left(\theta_i,\phi_i,\theta_s,\phi_s,\lambda_s\right)\right\rangle_{\Lambda_i=blue}\cdot\Delta\lambda_s}{\Delta\Lambda_s} \tag{12}$$

And with $\Delta\Lambda_s$ equal to the wavelength range of the emission spectrum. The TIS expression for the inelastic scattering becomes now:

$$TIS_{biys}=\sum_0^{2\pi}\sum_0^{\pi/2}\left\langle\left\langle q_e\left(\theta_i,\phi_i,\theta_s,\phi_s,\lambda_s\right)\right\rangle_{\Lambda_i=blue}\right\rangle_{\Lambda_s=yellow}\cdot\Delta\Lambda_s\cdot\cos\theta_s\cdot\sin\theta_s\cdot\Delta\theta_s\cdot\Delta\phi_s \tag{13}$$

The resulting TIS for this *biys* interaction is 26% for both backward and forward directions, respectively (Table 2).

5. Power budget

From Table 2 it can be concluded that when blue light is incident on the RPC, 37% of the total incident power is scattered backwards (11% blue light and 26% yellow light). Part of this backscattered light will be re-directed towards the RPC after reflection in the MC with an efficiency of approximately 94% (Table 1). This blue and yellow light will experience elastic scattering and wavelength conversion once again.

To obtain the total output of the LED module based on the measurement of the MC efficiency and the characterization of the RPC, an iterative model is introduced. The backward reflected light from the RPC, is reflected in the MC, back towards the RPC again. Again, a portion of the light will be sent back to the MC where it once more will be (partially) reflected to the RPC and so on. A schematic representation of the iterative model is given in Fig. 9.

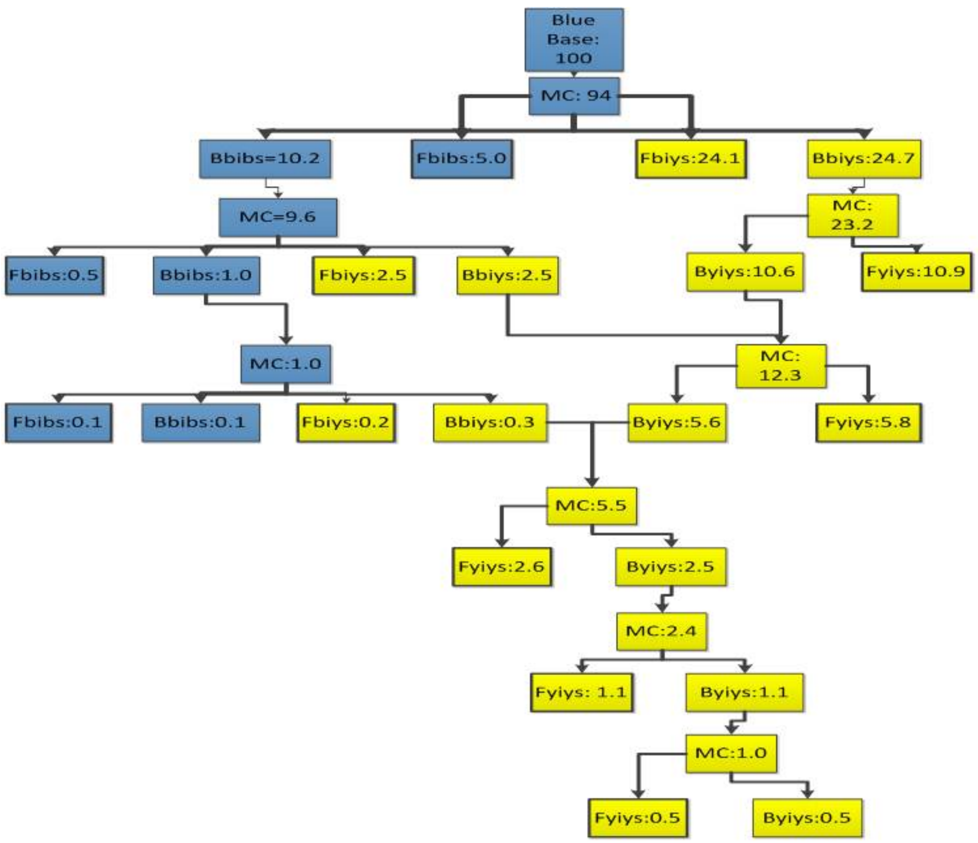

Fig. 9. Schematic representation of the iterative model and power budget calculations for the remote phosphor LED module.

Seven iterations of light being reflected between RPC and MC have been carried out to calculate the power budget of the complete module

The results are presented in Fig. 9 and Fig. 10. These values are based on BSDF values obtained for an average incident angle of 45°, although the MC induces several angles of incidence both for blue and yellow light.

Every forward contribution, escaping the LED module, is added to the total extracted power which is comprised by the blue extracted power and the yellow extracted power. At every iteration, the cumulative losses are calculated as well.

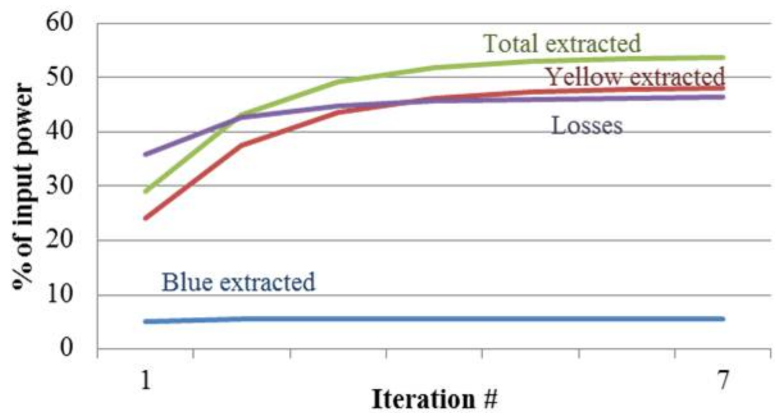

Fig. 10. Cumulative extracted power and losses in function of iteration.

It can be seen from Fig. 9 and Fig. 10 that the final cumulative losses account for 42.1% of the initial power, these are basically dissipated as heat in the RPC and the MC. The total cumulative extracted power of 57.8% of the initial power is composed of a blue contribution of 7.8% and a yellow contribution of 50.0%.

After the first iteration 29.2% of the input power escapes forward, and 36.0% is lost in: heat dissipation as a consequence of the Stokes shift, the quantum efficiency of the phosphor film and the absorption in the MC and the diffuser plate. The back-scattered power after the first interaction equals 34.8% (= 100-29.2-36.0), but after seven iterations only an extra 24.4% of the total input power escapes. Thus, around 10% of the input power is lost in the recycling process.

This two wavelength approach and the iterative simulation model are validated by measurements of the spectral radiant flux of the module. During measurements, the phosphor temperature does not exceed 40°C, which is below the thermal quenching limit for Eu doped phosphors, typically around 150°C [25]. Hence, the impact of the temperature rise on the optical characteristics can be neglected. The optical power of the module is measured and compared with the optical power of the blue LEDs mounted on the base. The spectral power is integrated over 450-470 nm to calculate the "blue power", while the integration over 470-740 nm constitutes the "yellow power" (See Table 3).

Table 3. Power budget comparison between results obtained through the iterative model and from measurements

	Blue extracted power [%]	*Yellow extracted power [%]*	*Total extracted Power [%]*	*Total Losses [%]*
Experiments	5.8	49.5	55.3	44.7
Iteration model ($\theta_i = 45°$)	5.6	48.0	53.6	46.4

From Table 3 it can be seen that iterative model agrees well with the experimental values. Deviations between model prediction and experimental values are below 4%. Even the blue/yellow ratio is predicted very well. The small mismatches may be attributed to the fact that the TIS power values have been calculated for only one incident angle (45°), which is indeed a simplification. However, the model allows the understanding of the powerful impact of the MC on the blue and yellow extracted light, as well as the main loss factors.

6. Photon budget

Additional to the power budget discussed in the preceding section, it is also interesting to discuss the photon budget of both the RPC and the complete remote phosphor module. Due to the wavelength conversion, power and photon flux are not always proportional.

When illuminating the RPC, the photon flux in the backward and forward directions is calculated in an analogous way to the power budget. For the interactions *bibs* and *yiys*, the photon ratio is the same as the power budget. In the *biys* case, however, the wavelength conversion induces a difference. In Eq. (13) the power fluxes $\Phi_{e,s}$ and $\Phi_{e,i}$ are converted in terms of photons according to Eq. (14) and Eq. (15):

$$\Phi_{e,s} = \Phi_{e,s}^{photons} \frac{\sum_{470}^{740} \Phi_{e,\lambda,s} \cdot h \cdot c \cdot \Delta\lambda}{\sum_{470}^{740} \Phi_{e,\lambda,s} \cdot \lambda \cdot \Delta\lambda} \tag{14}$$

$$\Phi_{e,i} = \Phi_{e,i}^{photons} \frac{\sum_{450}^{470} \Phi_{e,\lambda,i} \cdot h \cdot c \cdot \Delta\lambda}{\sum_{450}^{470} \Phi_{e,\lambda,i} \cdot \lambda \cdot \Delta\lambda} \tag{15}$$

With h the Planck constant, c the speed of light, and $\Phi_{e,s}^{photons}$ and $\Phi_{e,i}^{photons}$ the photon flux of the scattered and incident power, respectively.

Thus, inserting Eq. (14) and Eq. (15) into Eq. (13) results into the total integrated scattered photons given by Eq. (16):

$$\frac{\Phi_{e,s}^{photons}}{\Phi_{e,i}^{photons}} = \frac{\dfrac{\sum_{450}^{470} \Phi_{e,\lambda,i} \cdot h \cdot c \cdot \Delta\lambda}{\sum_{450}^{470} \Phi_{e,\lambda,i} \cdot \lambda \cdot \Delta\lambda}}{\dfrac{\sum_{470}^{740} \Phi_{e,\lambda,s} \cdot h \cdot c \cdot \Delta\lambda}{\sum_{470}^{740} \Phi_{e,\lambda,s} \cdot \lambda \cdot \Delta\lambda}} TIS_{biys} \tag{16}$$

The scattered photon ratios for each interaction are presented in Table 2. As expected, the photon budget for the *biys* interaction is much higher than the corresponding power budget. The photon budget only takes photon losses into account (due to the non-unity of the quantum efficiency of the phosphor and absorption in the diffusor), the power losses due to the wavelength conversion from high energy photons to lower energy photons (Stokes shift) are only accounted for in the power budget calculations.

From Table 2 it is also possible to calculate the external quantum efficiency of the RPC when blue light (peak wavelength: 460 nm; FWHM: 20 nm) impinges the material. The quantum efficiency is defined as the ratio of emitted ‘yellow’ photons (67%) to the blue absorbed photons (83%), and amounts to 80%, which is in close agreement with the values stated in literature [11,26].

6. Conclusions

A commercial RPC used in a remote phosphor LED module was characterized in terms of the BSDF in both reflection and transmission. Elastic scattering was defined by a spectral weighted average BSDF value for both blue and yellow wavelength regions. The wavelength conversion by the RPC was defined by an average weighted bi-spectral BSDF. Angular

#209148 - $15.00 USD Received 1 Apr 2014; revised 20 May 2014; accepted 21 May 2014; published 2 Jun 2014

integration of the BSDF values provided information on both power and photon fluxes of the RPC when illuminated with blue LEDs.

The RPC has been integrated in a remote phosphor LED module. The efficiency of the mixing chamber (MC), power and photon budget of the module were experimentally characterized by integrating sphere measurements.

An iterative model has been presented to determine the power and photon budget of an LED module based on the characterization by the BSDF values of the RPC and the efficiency of the MC. The model allows for identification of the most important loss factors. An excellent agreement between the iterative model and experimental results was found.

Although the recycling of backscattered light elevated the total extracted power to 73% compared with the extracted power after the first iteration, this could be further improved by reducing the losses not related to wavelength conversion.

Future work will include a full optical simulation of the unit taking into account particular angular variations and intensity distributions. This will allow for a very focused optimization approach of the light extraction in a module applying remote phosphor technology.

Acknowledgments

The authors would like to thank Prof. Philippe Smet from the Lumilab group in University of Ghent for his assessment in the excitation and emission spectra measurements. This research was partially supported by Colciencias (National Department of Science, Technology and Innovation - Colombia), the Flemish Hercules stichting (AKUL035) and the IWT (Flemish agency for Innovation by Science and Technology).